RSC Advances

PAPER

View Article Online
View Journal | View Issue

Cite this: *RSC Adv.*, 2025, **15**, 7786

Onion peel derived carbon nanoparticles incorporated polysulfone membranes: enhanced dye removal from water†

Aman Sharma, [ab] Soumi Datta, [c] R. K. Sanjana,[b] B. M. Pooja,[b] Suryasarathi Bose [c] and Gurumurthy Hegde *[ab]

The ongoing discharge of hazardous dyes from industrial processes has intensified global water pollution, posing serious threats to aquatic ecosystems and human health. Addressing this challenge, our study explores the potential of bio-based carbon nanomaterials (CNM), synthesized from onion peel biowaste and designated as ON11, as effective agents in dye removal. These CNMs were incorporated into a mixed matrix membrane (MMM), using polysulfone (PSU) as the membrane substrate, to enhance dye adsorption. The CNM synthesis was achieved through a simple, eco-friendly process. We examined their impact on adsorption efficiency by introducing ON11 nanoparticles at varying concentrations into the PSU membrane (ON11@PSU). This CNM-embedded membrane structure offers a solution to challenges associated with the large-scale application of nanomaterials, particularly by minimizing leaching into water and improving durability. The ON11 and ON11@PSU membranes were characterized using various techniques, including SEM, Raman spectroscopy, XRD, optical profilometer, and FTIR, to confirm their behavior, morphology, and structural integrity. The surface area of ON11 was 423.26 $m^2\ g^{-1}$, with BJH average pore diameter of 4.5 nm and BET pore volume of 0.26 $cm^3\ g^{-1}$. ON11 nanoparticles were adsorptive in nature, and their utility in membrane adsorption is explored. The influence of parameters, including contact time, dye concentration, membrane thickness, pH, and adsorbent dosage, was systematically evaluated to optimize the dye adsorption efficiency of the ON11@PSU membrane pad. It was observed that the thickness of the 60 μm membrane (S_a = 2.170 μm and S_q = 2.75 μm) showed higher removal efficiency for all the selected dyes than the other thicknesses at the native pH itself. The MMM demonstrated its effectiveness as an adsorbent membrane, achieving maximum removal efficiencies of approximately 98% for MG dye, 92% for RhB dye, and 67% for MB dye. The negative zeta potential of adsorptive membranes enabled the electrostatic attraction of positively charged dyes, enhancing adsorption capacity. The findings contribute to developing sustainable and effective membrane utility as adsorbents, opening avenues for the effective use of agricultural waste products in environmental remediation applications.

Received 2nd January 2025
Accepted 28th February 2025

DOI: 10.1039/d5ra00025d

rsc.li/rsc-advances

1. Introduction

In recent years, the increasing global demand for textiles, pharmaceuticals, and various industrial processes has led to an alarming increase in the discharge of synthetic dyes into aquatic ecosystems. Water pollution caused by low utilization efficiency and uncontrollable discharge of organic dyes has greatly harmed the ecological environment and biological survival, resulting in a significant potable water deficit. In view of this, the global freshwater demand will be 40% higher than supply by 2030.[1] The enduring presence of these dyes presents a major environmental hazard, underscoring the pressing need for sustainable and efficient wastewater treatment methods.[2] Dyes like methylene blue (MB), malachite green (MG), and rhodamine B (RhB) pose a significant threat to the environment, humans, and aquatic organisms.[3] Methylene blue is a cationic dye whose toxicity renders it hazardous to human health above a specific concentration.[4,5] Long-term exposure to it may result in nausea, vomiting, anemia, and high blood pressure.[6] Malachite green is a cationic, crystalline dye that is soluble in water and is highly utilized in the industrial and manufacturing sectors that produce silk, paint and pigment, food, textile dying, leather, paper, *etc.* It is carcinogenic, teratogenic, mutagenic, and persistent in nature.

[a]*Department of Chemistry, School of Sciences, Christ University, Bengaluru, 560029, Karnataka, India. E-mail: murthyhegde@gmail.com*

[b]*Centre for Advanced Research and Development (CARD), Christ University, Bengaluru, 560029, Karnataka, India*

[c]*Department of Materials Engineering, Indian Institute of Science, Bengaluru, 560012, Karnataka, India*

† Electronic supplementary information (ESI) available. See DOI: https://doi.org/10.1039/d5ra00025d

When ingested through water by humans, it damages the heart, kidneys, and organs.[7,8] On the other hand, RhB is a red alkaline xanthene dye used extensively in food, paints, inks, fabrics, and pens because of its non-biodegradability, water solubility, and stability. Wastewater contaminates surface water, causing health and environmental problems such as respiratory, skin, and eye irritation, nervous system damage, and carcinogenic impacts.[9,10]

Wastewater-containing dyes have been treated using a wide range of physical, chemical, and biological techniques, such as membrane filtration, adsorption, biosorption, coagulation/flocculation, advanced oxidation, photocatalytic degradation, phytoremediation, electrolytic treatment.[6,11,12] Although these techniques have their own advantages and limitations. Adsorption, in contrast, has emerged as an alternative pollution detoxification method due to its low cost, effectiveness, sustainability, and convenience of use.[7,9] Despite advances in particle adsorbents, their large-scale application for dye removal meets obstacles such as difficult separation and recovery, adsorbent loss, and issues with high-pressure drop and poor flow rate in packed-bed procedures.[11] The separation process based on extraction requires a significant amount of solvents to remove organic contaminants. Membrane procedures provide an alternative to traditional separation approaches for overcoming this issue.[13] Adsorptive membranes with adsorptive qualities have emerged, and research is being performed to increase dye rejection at low production and operational costs. Incorporating adsorbents into a polymer matrix of a substrate enhances dye rejection by capturing dye molecules through hydrogen bonding and electrostatic interactions, effectively preventing their passage through the membrane.[14] Incorporating particulate adsorbents into separation membranes successfully solves the disadvantages of classical adsorbents. Classical adsorbents, such as powders or granules, often face limitations such as low reusability due to challenges in recovery and reuse, inefficient mass transfer caused by agglomeration or poor dispersibility in water, and high energy and cost requirements for post-adsorption separation processes like filtration or centrifugation. Incorporating particulate adsorbents, such as the *Allium cepa* peel-derived CNM in our study, into separation membranes successfully addresses these issues. The thin membrane walls (micron size) minimize packed bed height, increasing flow rates and minimizing pressure drops while removing the need for further adsorbent separation and recovery.[11]

Different materials, like Fe_3O_4/sulfonated graphene oxide (SGO),[14] arginine arginine-modified montmorillonite,[15] polyvinylpyrrolidone (PVP)–SiO_2,[16] *etc.*, have been utilized to date in membranes for dye adsorption. Almost all parts of plant wastes could be used as adsorbents because they contain –COOH, –OH, or phenolic groups that could provide several types of bindings (*e.g.* charge interaction, hydrogen bonding, or hydrophobic interaction).[17] Although there is no report to date on utilizing biomass-derived carbon nanospheres (CNS) into membranes for dye adsorption. Biomass-derived CNSs are mesoporous and have a spherical shape, making them a suitable candidate for dye degradation applications. CNSs have emerged as intriguing candidates for enhanced environmental remediation techniques due to their unique physicochemical features and abundance of surface functionalities.[18] Also, the use of biowaste-derived nanomaterials helps to realize circular economy objectives as they allow the transformation of waste streams into high-added-value materials.[19]

The current study investigates a novel technique to address dye removal issues using carbon nanospheres generated from onion peels and embedding them in polysulfone (PSU) membranes. The PSU polymer was utilized for this study due to its excellent thermal and chemical stability, high mechanical strength, and ease of processing, which make it suitable for wastewater treatment applications. Additionally, PSU is cost-effective and widely available, offering an optimal balance of performance and scalability compared to higher-performance polymers. These factors align well with the objectives of our study and the practical feasibility of scaling up the developed membranes. Onion peels, an agricultural waste product, have received attention for their high carbon content and distinctive structural characteristics. Carbon nanospheres are derived from onion peels through a sustainable and cost-effective synthesis process, presenting a green, eco-friendly alternative for environmental applications.[20] By integrating onion peel-derived carbon nanospheres into membranes, the adsorption parameter for the removal of synthetic dyes in wastewater is evaluated. Membrane-based technologies are flexible and can be synthesized on a large scale for water treatment purposes, and such treatment is efficient and has a low environmental impact.[21] This work examines the combination of carbon nanospheres and membranes to increase dye adsorption, assist in the separation, and enable the breakdown of difficult dye molecules. It is envisaged that the present study will provide useful information on the advancement of wastewater treatment systems in an eco-friendly and sustainable manner to reduce the adverse impact of synthetic dyes on the environment.

2. Experimental section

2.1. Materials and reagents

The raw material precursor-*Allium cepa* (Onion) peels was collected from southern India (Karnataka) to synthesize CNM. The dried peels were ground to a fine powder using a Bajaj Rex mixer grinder. The tube furnace from NoPo Technologies was used for the pyrolysis process. Methylene blue (MB), malachite green (MG), and rhodamine b (RhB) dyes were procured from Sigma-Aldrich. Sodium hydroxide (NaOH) from CDH and hydrochloric acid (HCl) were procured from Thomas Baker. *N*-Methyl-2-pyrrolidone (NMP) was used as a solvent from Finar Pvt. Ltd. For the recyclability test, ethanol was used as a solvent. Polysulfone (PSU) was used as a membrane polymer procured from Sigma-Aldrich. Millipore water from Milli-Q, Progard® TS2 was used for all the studies.

2.2. Synthesis of matrix mixed membrane pad (ON11@PSU-pad)

2.2.1. Synthesis of carbon nanomaterial (CNM). *Allium cepa*-derived CNMs were synthesized using the one-pot pyrolysis

technique by our group.[22] The onion peels obtained were cleaned manually to remove debris, rinsed with distilled water, dried in the open air, and then sunlight dried. The waste water after washing was collected and reused for gardening to maintain sustainability. The dry onion peels were ground and finely powdered. Next, the powder was run through a sieve with pores about 75 μm in size and pyrolyzed at 1100 °C under a nitrogen atmosphere with a heating rate of 10 °C min^{-1}. The yield obtained was approximately 35% from this process. During pyrolysis, the different components of the precursor were degraded at various temperatures in the inert atmosphere. Moisture and water content were eliminated at ~105 °C from the biowaste. Volatile compounds like CO_2, CH_4, and CO were released with the decomposition of hemicellulose at 220–315 °C. Cellulose degraded at a further temperature of 315–400 °C, and lignin degraded slowly in a wider range from ambient to 900 °C.[23] The carbon-rich residue that is well-defined, spherical, and porous in nature occurs at high temperatures. The temperature was then elevated to 1100 °C for complete pyrolysis, and then the synthesized nanoparticle was washed with 1 M HCl, followed by distilled water, and dried. Hereafter labeled as ON11 in the manuscript.

2.2.2. Preparation of carbon nanomaterial-infused membrane-pad (ON11@PSU-pad). ON11@PSU-pad membranes with different weight percentages of CNS were prepared using the Nonsolvent-Induced Phase Inversion (NIPS) method. The desired amount of CNS was added to 16 mL of NMP and sonicated for 30 min to achieve uniform dispersion of CNMs, followed by stirring (constant speed and temperature). The amount of ON11 nanoparticles is tabulated in wt% in Table 1. When the temperature reached ~60 °C, around 4 g of PSU was slowly added to the above solution and stirred overnight.[24] The viscous solution was cast onto a glass plate with the Doctor Blade using different casting thicknesses of 120 μm, 90 μm, 60 μm, and 30 μm. After that, the glass plate was submerged in a distilled water coagulation bath to create a composite membrane sheet. The membranes were immersed in a water bath for 24 h, air-dried, and used. For subsequent experiments, the membranes were shaped into standard spherical-sized tokens. The graphical representation of the preparation method is described in Scheme 1.

2.3. Materials characterization techniques

The morphology of ON11 and ON11@PSU membranes was analyzed using Scanning Electron Microscopy (Apreo 2S Thermoscientific and Zeiss). The surface functionalities were analyzed using the Fourier Transform Infrared Spectroscopy (FTIR) technique using Shimadzu IRSpirit. Raman spectra were analysed using a Renishaw inVia Raman microscope for information about the crystalline structure. Using a MiniFlex 600 from Rigaku Corporation, X-ray diffraction (XRD) patterns are used to assess the crystallinity of material. Brunauer–Emmett–Teller (BET) method was used to estimate surface area and pore size distribution using BELSORP MINI X, Japan at 77K N_2 adsorption. An optical profilometer was used to calculate the surface roughness and topology of the ON11@PSU-pad membranes. The zeta potential of the ON11 was analyzed by Malvern Zetasiezer ZEN3600 Particle Analyzer. The absorbance of the dye concentration was noted using a UV-visible spectrophotometer (Ocean Optics).

2.4. Dye adsorption experiments

The membranes were cut into standard-sized tokens to check the dye removal efficiency. One parameter was modified to assess the impact of other factors, including membrane thickness (30–120 μm), adsorbent dosage (0.024–0.073 wt%), contact period (10–70 min), and dye concentration (2.5–7.5 ppm). The rest of the parameters were considered constant. The effects of contact time, pH, membrane thickness, dye concentration, and nanoparticle dosage on dye adsorption were studied in detail. The studies were carried out in three trials, and the average error percentage is shown. Furthermore, the optimized parameters from the previous stage were used to study the effect of another parameter. The experiment was carried out in a beaker with a constant stirring rate, keeping the token membrane at the bottom. The physicochemical characteristics of the selected dyes is mentioned in Table 2. The absorbance before and after the contact time is checked using a UV-vis spectrophotometer, and the removal efficiency is calculated using eqn (1).

$$\text{Removal efficiency}(\%) = \frac{C_e - C_0}{C_e} \times 100 \quad (1)$$

C_0 and C_e are the dye concentrations under initial and equilibrium conditions.

Pseudo-first and pseudo-second order kinetic studies were performed and these models were fitted using linear square fitting in the Origin Pro 9.0 64-bit software.

3. Results and discussion

3.1. Physiochemical characterization of ON11 and ON11@PSU

3.1.1. FESEM analysis. SEM analysis reveals the surface and cross-section morphology of the membrane, as depicted in

Table 1 Composition of membranes in weight percentage

CNS dosage in membrane (mg)	PSU (wt%)	NMP (wt%)	ON11 (wt%)	Refer as
—	19.53	80.46	—	PSU
5	19.53	80.45	0.024	ON11-5@PSU
10	19.52	80.43	0.048	ON11-10@PSU
15	19.51	80.41	0.073	ON11-15@PSU

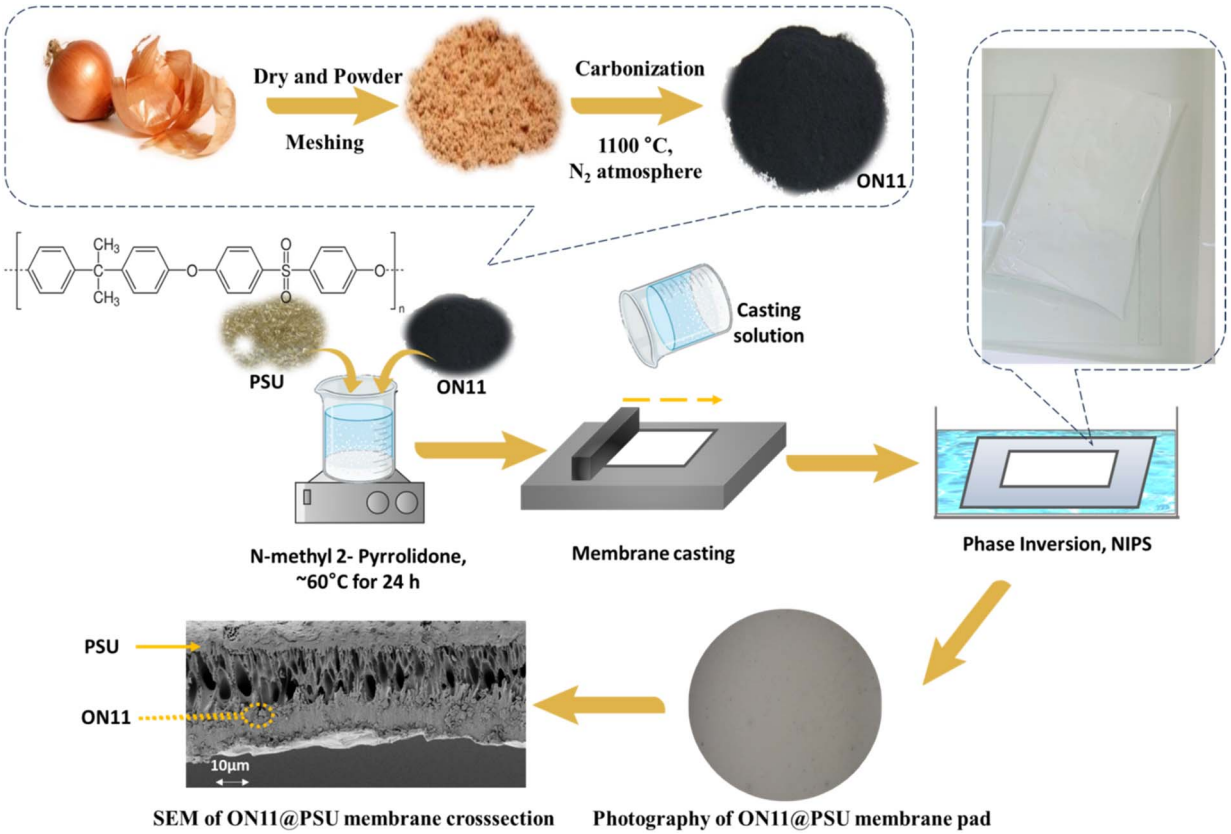

Scheme 1 A graphical description of the carbon nanomaterial (ON11) production process, followed by the development of a mixed matrix membrane (ON11@PSU-pad) employing the nonsolvent-induced phase separation (NIPS) technique.

Fig. 1. The ON11 nanoparticles showed around 70% carbon using EDS, confirming the formation of carbon nanospheres, as illustrated in Fig. 1a. The unmodified PSU membrane exhibits evident asymmetry and porosity with a denser skin layer on the surface, accompanied by finger-like macrovoids,[25] as seen in Fig. 1e. The interfacial region has a estimated height of around 10.65 μm (refer to ESI Fig S1† for magnified interfacial SEM image). The structural characterization presented in this study demonstrates the unique elements of the membrane, thus acceding to the understanding of its composition and architecture. Fig. 1c and d of the surface morphology of the ON11-10@PSU-pad is shown before and after dye adsorption, indicating that the dye molecules are adsorbed in clusters on the surface.

3.1.2. FTIR assessment. The functional groups present in the biomass precursor, synthesized nanoparticles, and

Table 2 Physicochemical characteristics of MB, MG, and RhB dyes

Parameter	Methylene blue (MB)	Malachite green (MG)	Rhodamine B (RhB)
Chemical formula	$C_{16}H_{18}ClN_3S$	$C_{23}H_{25}ClN_2$	$C_{28}H_{31}ClN_2O_3$
Molar mass	319.85 g mol^{-1}	364.91 g mol^{-1}	479.02 g mol^{-1}
Types of ion	Cationic	Cationic	Cationic
Maximum wavelength (λ_{max})	~665 nm	~617 nm	~554 nm
Chemical structure	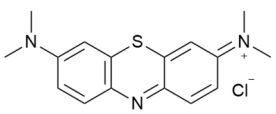	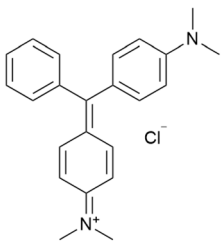	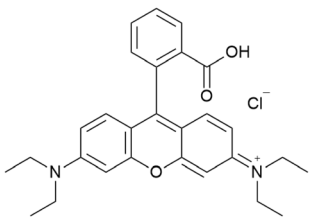

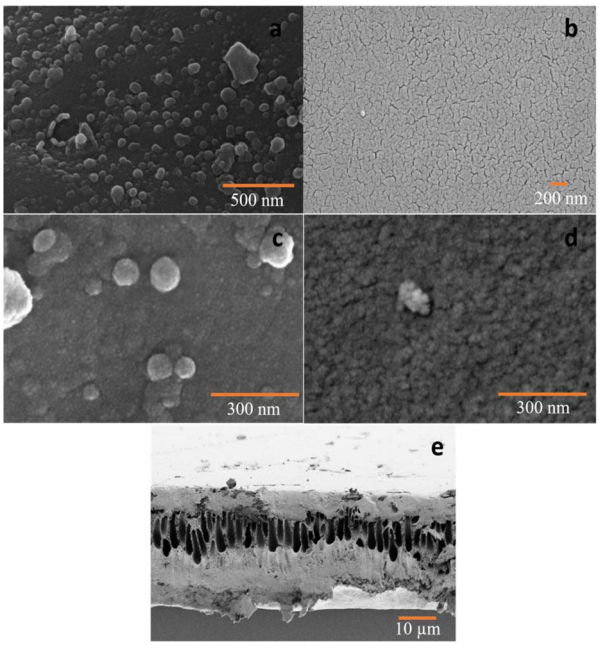

Fig. 1 SEM images of the (a) ON11 nanoparticles, (b) surface morphology of pristine PSU, (c) ON11-10@PSU-pad, (d) ON11-10@PSU-pad after dye adsorption, (e) the cross-section of the PSU membrane.

membrane are analyzed by FTIR spectroscopy. Fig. 2a represents the functionalities present in the precursor and ON11 CNS. Before pyrolysis, the broadband at 3260 cm^{-1} represents the O–H stretching vibrations caused by the water molecules in the precursor. The band at 2906 cm^{-1} is due to the C–H stretching vibrations. The C–H vibrations due to the presence of aromatic compounds are attributed to 2078 and 1907 cm^{-1}. The strong bands at 1604 and 1004 cm^{-1} represent C=C stretching and bending vibrations caused by carboxylic acid and alkene, respectively.

After pyrolysis, the band at 2980 cm^{-1} corresponds to the hydroxyl group present. The stretching vibrations at 2335 cm^{-1} are caused by ambient CO_2 adsorbed on the nanoparticles.[26] Alkyne and allene (C=C=C) groups are represented by the 2101 and 1970 cm^{-1} bands, respectively. The band at 1440 cm^{-1} represents the methylene (C–H) group attached to the synthesized carbon nanospheres. The decrease in intensity is attributed to the degradation of the precursor during pyrolysis.[27]

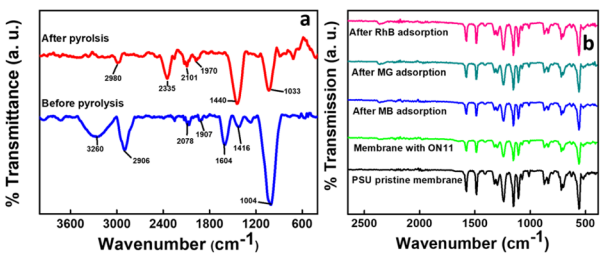

Fig. 2 FTIR analysis of (a) ON11 CNS before and after pyrolysis, (b) ON11-10@PSU-pad before and after adsorption of respective dyes.

In the FTIR spectrum of the ON11@PSU membrane, as depicted in Fig. 2b, the peak at 1239 cm^{-1} is attributed to the stretching vibration of the C–O–C groups. The skeletal vibrations of aromatic hydrocarbons are associated with the peaks at 1484 and 1576 cm^{-1}, while the symmetric and asymmetric stretching of sulfone groups are associated with the peaks at 1153 and 1325 cm^{-1}. The peak at 560 cm^{-1} corresponds to a strong halogen bond (Cl^-), and the peak at 1107 cm^{-1} to medium C–N stretching.[28]

3.1.3. XRD and Raman analysis. XRD gives the crystallographic structure of the sample. From the XRD pattern (Fig. 3a), a broad peak around 2θ ~24° and a sharp peak at 2θ ~29° corresponding to d_{002} show interlayer spacing of graphitic carbon, which is also attributed to silicon impurities present in the synthesized ON11 nanoparticles. Another peak at 2θ ~43° shows in-plane diffraction corresponding to d_{100}, which is characteristic of the carbon nanospheres. The smaller shoulder peaks around 2θ ~47° can be visualized. Overall, the pattern suggests that the nanoparticles synthesized are semi-crystalline and partially amorphous in nature.

The XRD pattern of ON11-10@PSU membrane before and after dye adsorption is shown in Fig. 3b. The decrease in the peak intensity is observed after the dye adsorption, without any other significant changes in the pattern. The outcome implies that the dye-adsorbed carbon nanospheres might not induce the bulk phase shifts.[29] It suggests that the membrane is amorphous. Additionally, the Raman spectrum (Fig. 3c) reveals the presence of a D-band, indicating structural defects and disorder within ON11, while the presence of a G-band confirms the sp^2-hybridized carbon network characteristic of its graphitic structure. The intensity ratio of these bands was measured at 0.84, with the G-band observed at 1598 cm^{-1} and the D band at 1349 cm^{-1}.[30,31]

3.1.4. Optical profilometry analysis. The surface topography images of ON111-10@PSU-pads were analyzed by the Optical Profilometer. Fig. 4a–d are the membranes with various thicknesses (30, 60, 90, and 120 μm), suggesting the irregularity on the surface of membranes (refer to ESI Fig. S2† for 2D optical profilometry images of the respective thickness). In Fig. 4a, the surface is relatively flatter compared to others. Fig. 4b indicates that the 60 μm membrane has more surface roughness than the thinner (30 μm) membrane. Surface roughness increases effective surface area, creating more active places for dye molecules to interact. The peaks and valleys are anticipated to enhance the number of contact points between the membrane and the dye solution, enhancing adsorption capacity. Fig. 4d shows a similar surface to Fig. 4c but with smoother parts alternating with rough patches. The surface could result from membrane thickness, where nanosphere dispersion becomes uniform, possibly due to sedimentation or aggregation at increasing thicknesses. However, if the thickness of the membrane is less, it is better for adsorption, but the very thin membrane would also be delicate, leading to less stability. Thereby, the 60 μm membrane is selected for further studies.

Using an optical profilometer, surface roughness can be calculated, which is the average roughness (S_a) that is defined as

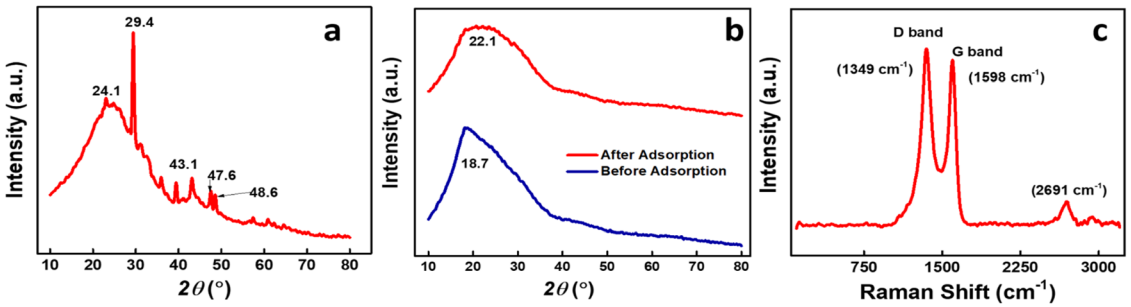

Fig. 3 XRD analysis of (a) ON11, (b) ON11-10@PSU-pad before and after dye adsorption, and (c) Raman spectra of ON11.

the average height of all measured locations in the measurement.[32] Eqn (2) contains the formula for calculating it.

$$S_a = \frac{1}{A}\iint_A |Z(x,y)|\mathrm{d}x\mathrm{d}y \quad (2)$$

where, S_a = average surface, A = total area and $Z(x,y)$ is the height of each point (x,y). The data indicates that the 60 μm ON11-10@PSU membrane pad exhibits the highest surface roughness (S_a) value at 2.170 μm, suggesting a more textured surface compared to other pads. Increased surface roughness, characterized by deeper valleys and higher peaks, enhances the likelihood of dye molecules staying in contact with the membrane for extended periods, facilitating greater adsorption. The S_a values for the 30 μm, 90 μm, and 120 μm membranes were recorded at 0.717, 0.606, and 0.770 μm, respectively—significantly lower than the 60 μm membrane. Additionally, the root mean square roughness (S_q) values for these membranes were 0.911 μm, 2.75 μm, 0.783 μm, and 0.964 μm, respectively. The peak-to-valley height (S_{pv}) was highest for the 60 μm membrane, measuring 34.11 μm.

3.2. Application of ON11@PSU-pad in organic pollutant adsorption

3.2.1. Adsorptive behavior of different compositions of ON11@PSU. The adsorption experiments were conducted using varying doses of standalone ON11 nanoparticles, a membrane composed solely of PSU, and mixed matrix membranes (MMM) incorporated with ON11 nanoparticles. The results, presented in Fig. 5a, show that increasing the ON11 dosage significantly enhanced dye removal efficiency in a shorter time. At an adsorbent dosage of 0.5 g L^{-1} (ON11-5), approximately 97.5% dye removal was achieved within 5 minutes. At 1 g L^{-1} (ON11-10) ON11 dosage, the removal efficiency reached nearly 99.8% in less than 20 seconds, demonstrating the superior performance of ON11 as an adsorbent in dye removal applications. The high adsorption efficiency of ON11 is attributed to its abundant active sites,[33,34] whereas the PSU membrane alone was ineffective in adsorbing dye molecules. When incorporated into the MMM, ON11 significantly improved dye removal, specifically for MG dye. The pristine PSU membrane showed only 20% removal after 60 minutes, while the ON11@PSU membrane achieved more than 91% removal in the same time frame. These

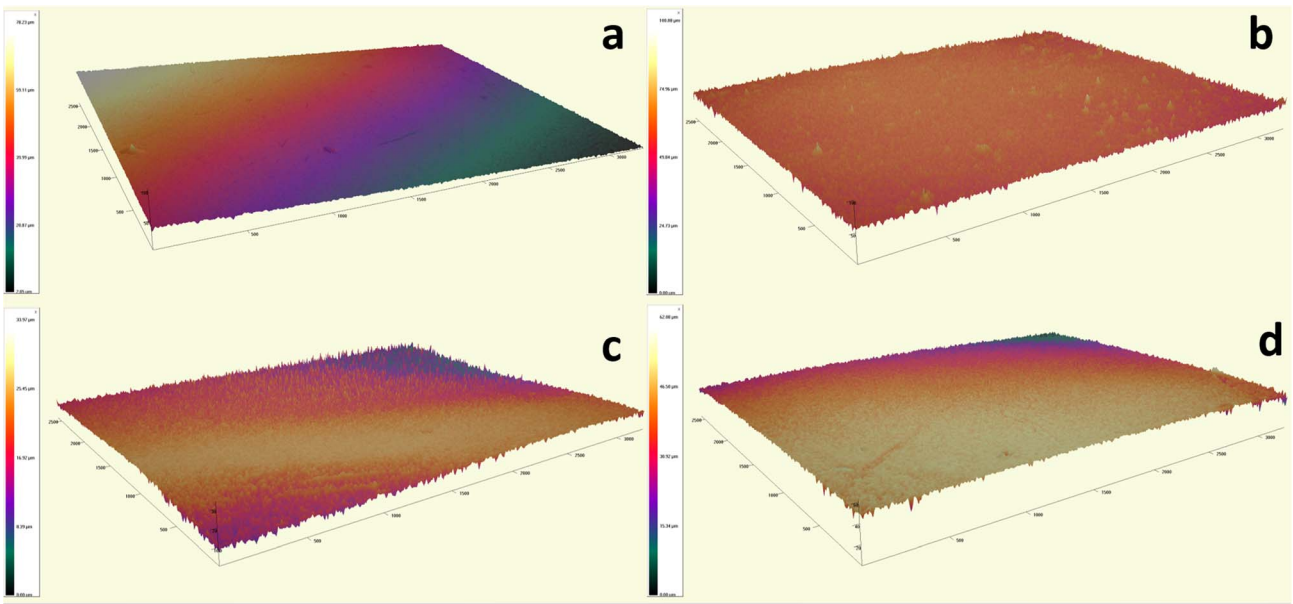

Fig. 4 Optical Profilometry 3D-image of ON11-10@PSU pad at different thickness (a) 30 μm, (b) 60 μm, (c) 90 μm, and (d) 120 μm.

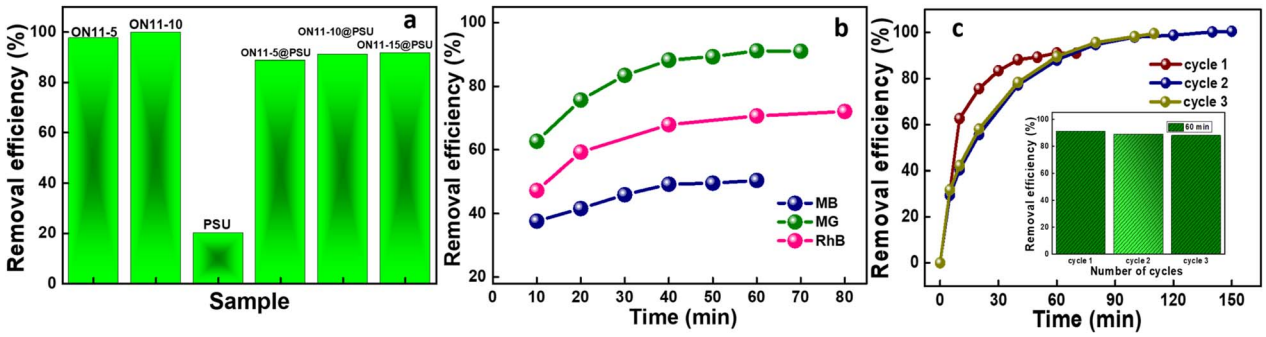

Fig. 5 (a) Comparison of different dosages of ON11 as adsorbent itself and in membranes; (b) contact time studies of cationic dye removal with ON11-10@PSU-pad; (c) recyclability test using MG dye.

Table 3 Comparative data for removal of cationic dyes using different MMMs

Dye	Polymer	Carbon type	Method	Removal efficiency (%)	Time (min)	Ref.
RhB	PSU + PVP (DMF solvent)	CNS synthesized hydrothermally	Ultrafiltration	81.5	—	35
CR	PSU (DMF solvent)	30% activated carbon	Ultrafiltration	99.5	360	36
RhB	PSU	Aluminium and gallium hybrid	Ultrafiltration	80	—	37
MB	PSU	Activated carbon spheres (resorcinol and formaldehyde)	—	99.9	—	38
RhB	Polydopamine (hexane solvent)	Silk nanofibrils-MOF composite	Adsorption	99.5	—	39
MB	PSU (NMP solvent)	CNS from biowaste synthesized *via* pyrolysis	Adsorption	67	60	This work
MG				98		
RhB				92		

findings highlight the enhanced dye adsorption performance of the MMM, making it suitable for large-scale applications. Additionally, embedding the nanoparticles into membranes addresses the challenge of nanoparticle recovery after dye adsorption, as it simplifies the process. In subsequent experiments, ON11-10@PSU membranes were further tested to evaluate their performance under different conditions. Table 3 shows comparative dye removal with other MMM from recent literature.

3.2.2. Effect of contact time and number of ON11-10@PSU-pads on adsorption. To assess the equilibrium time and determine how rapidly the pollutant is adsorbing on the adsorbed surface, contact time analysis is crucial for adsorption studies. In light of this, the study investigated contact times between 10 and 70 minutes under ideal circumstances (dye concentration: 5 ppm, volume: 10 mL, at room temperature ~28 ± 2). Fig. 5b shows that the proportion of dye removal increased with extended contact durations and stabilized after 60 minutes. It can be observed that the removal efficiency of dye increases with an increase in time. After a specific time frame, it remains constant or decreases as it reaches saturation. This is due to the maximum adsorption at the active sites of the membrane and saturation of the binding sites.[40,41] As more ions are adsorbed into the membrane matrix, steric hindrance increases and active sites decrease.[42] In this study, the maximum dye removal efficiency was observed at 60 minutes of contact time, with equilibrium reached for all the dyes with one layer of ON11-10@PSU-pad. The removal efficiencies were ~48 ± 8% for MB, ~91 ± 3% for MG, and ~76 ± 4% for RhB (all dyes with 5 ppm concentration). Additional experiments were conducted using two and three layers of ON11-10@PSU-pads for MB dye removal to assess their variation of removal efficiency. The results showed that, under the same experimental conditions, the removal efficiencies were ~74.7% and ~80.9%, respectively for MB dye. These findings indicate that adding more layers of ON11@PSU increases the contact area for adsorption, thereby improving dye removal. This affirms that the adsorption process is highly efficient and dependent on the availability of adsorptive sites for the dye molecules. Multiple layers of membranes would exhibit higher adsorption capacities in a shorter time duration, making them more effective for large-scale applications.

3.2.3. Effect of ON11@PSU-pad thickness study. The removal efficiency of the ON11@PSU-pad was evaluated at four different thicknesses for MB, MG, and RhB dyes. For MB, the removal efficiencies were 30 μm = 40 ± 8% < 60 μm = 47 ± 8% > 90 μm = 30 ± 7% > 120 μm = 36 ± 6%. This data suggests that the removal of MB dye is greater with thinner membranes (30 μm and 60 μm). Higher removal efficiency at low thicknesses might be due to improved diffusion of dye molecules through thinner membranes, which leads to better interaction with nanoparticles followed by the active membrane sites. For a thicker membrane pad, molecular structure of MB may cause it to interact differently with the membrane material, affecting adsorption efficiency[43] (refer to ESI Fig. S3† for thickness variation of membranes of respective dyes removal and Fig. S4† for

real membrane images dor adsorption of the selected dyes). In comparison, the removal efficiencies for MG were higher, *i.e.*, 78 ± 8%, 91 ± 3%, 56 ± 5%, and 74 ± 4% for the corresponding thicknesses recorded, indicating that dye removal was best around a membrane thickness casting of 60 μm (Fig. 6a). The removal efficiency of RhB was stable at around 70 ± 5%, 77 ± 4%, 48 ± 9%, and 70 ± 5% for increasing thickness, respectively. Across all dyes, the thickness of 60 μm ON11-10@PSU-pad demonstrated the best performance, possibly due to an appropriate surface area, thickness, and availability of the active regions for adsorption. In thicker membranes (120 μm), there may be a trapping or re-adsorption effect in which dye molecules enter the ON11@PSU pad and cannot quickly exit, increasing the observed adsorption. The phenomenon is less noticeable at 90 μm due to insufficient interconnected pore networks. However, it may become prominent in 120 μm wherein the membrane topology increases retention or re-adsorption in deeper layers.[44,45] Based on these results, the 60 μm membrane was chosen for further studies due to its favorable topography and surface roughness characteristics.

3.2.4. Effect of dye initial concentration on adsorption performance using ON11@PSU-pad. The concentration of the three dyes stated above was adjusted, and their removal efficiency was calculated at a contact period of 60 minutes. The dye removal efficiency of the membrane depends on the number of sorptive sites available on it.[46] As the concentration of the dye increases, more and more dye molecules occupy these sites. The dye removal efficiency of the membrane decreases as the concentration increases due to the saturation of the sorption sites in the membrane.[47] As seen in Fig. 6b, removal efficiency for 2.5 ppm concentration of MB dye was 67 ± 5%, whereas after doubling the concentration, it decreased to 48 ± 8%, and on a further 7.5 ppm dye concentration, it was 43 ± 3%. Similarly, the trend was observed in the other two dyes. For MG, removal efficiency decreased from 98 ± 3% to 78 ± 3% on increasing the dye concentration from 2.5 ppm to 7.5 ppm. For RhB, removal efficiency decreased from 92 ± 3% to 66 ± 4% on increasing the dye concentration from 2.5 ppm to 7.5 ppm. In other words, raising the concentration of the dye by a particular level raises the number of unoccupied sites of the adsorption that attract the dyes.[48] At higher initial dye concentrations, the total number of accessible adsorption sites is limited, potentially reducing the percentage of dye removed. The rise at higher concentrations could be related to increased driving force[49,50] (refer to ESI Fig. S5† for contact time study with dye initial concentration).

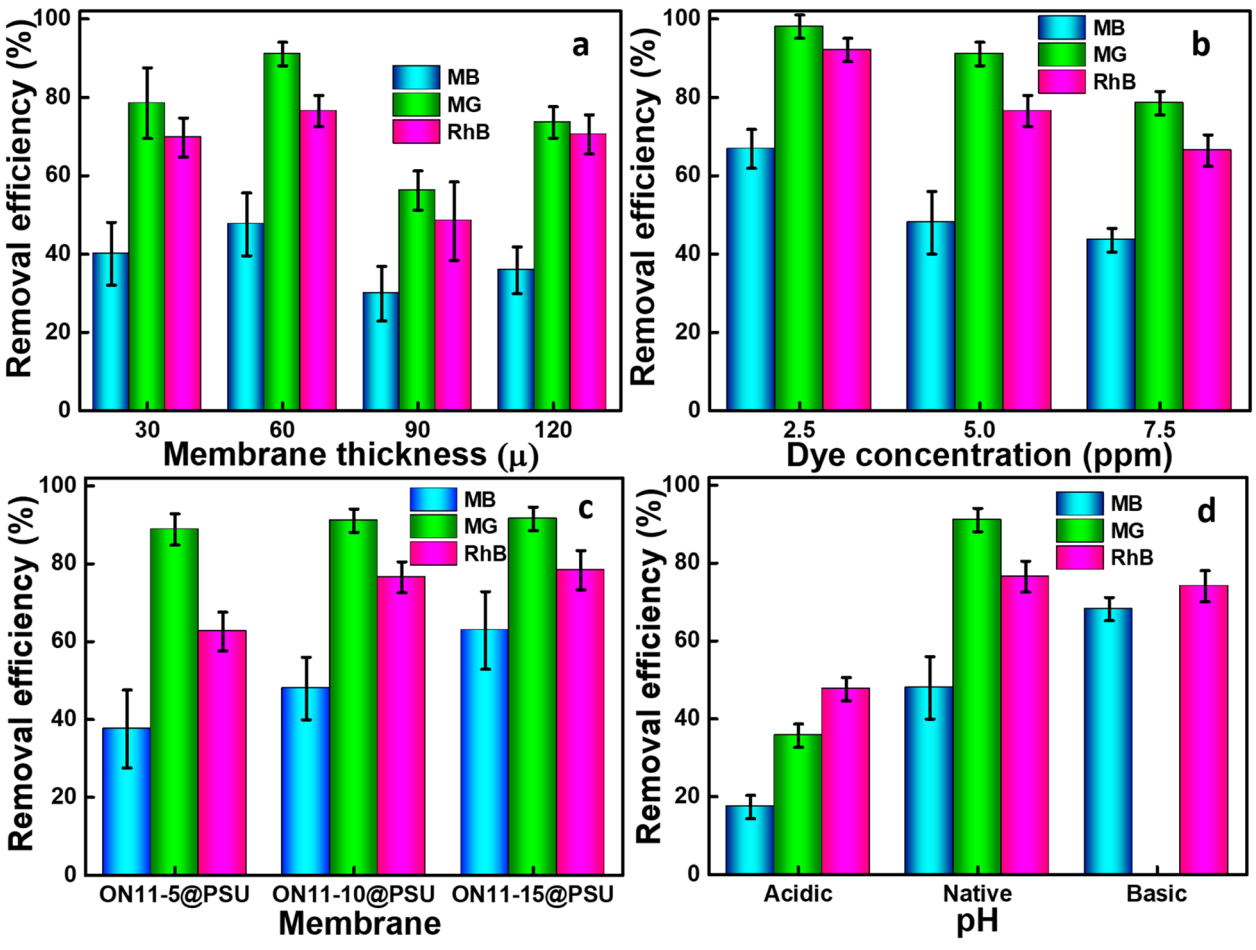

Fig. 6 Effect of (a) membrane thickness, (b) dye concentration, (c) ON11 dosage in membrane, (d) pH of dye solution for dye removal with ON11@PSU-pad.

3.2.5. Effect of ON11 dose study on ON11@PSU-pad. The amount of adsorbent used determines the rate at which contaminants are removed from aqueous solutions.[51] It is observed that an increase in the amount of nanoparticle dosage will increase the dye removal efficiency, but high doses of the nanoparticle will increase the aggregation, which will decrease the surface area and the sorptive sites, hence decreasing the dye removal efficiency.[52] However, molecular structure/weight of dye, surface charge, and adsorption behavior are vital in adsorbent–adsorbate interaction. Fig. 6c shows the dye removal efficiency for different doses of nanoparticles in the membrane as calculated in Table 1. For MB, MG, and RhB, the removal efficiency for ON11-5@PSU-pad was around 37 ± 10%, 89 ± 4%, and 63 ± 5%, respectively, whereas, for ON11-15@PSU-pad, it was 63 ± 10%, 91 ± 3%, and 78 ± 5%, respectively, for the selected dyes. For, ON11-10@PSU-pad, the removal efficiency was noted at 48 ± 8%, 91 ± 3%, and 76 ± 4%, respectively (refer to ESI Fig. S6† for ON11 dosage on dye removal study with respect to time on ON11-5@PSU, ON11-10@PSU, and ON11-15@PSU-pad membranes).

The membrane adsorption of dyes may be mediated by chemical bonding or interactions, such as electrostatic forces or hydrogen bonding, which make it less susceptible to the surface area offered by ON11 nanoparticles. As observed from the data above, the higher ON11 dosage shows a high removal efficiency of the dye as it provides more absorption sites.[53–56] This trend is consistent with findings from adsorption experiments, where increasing adsorbent dosage results in a bigger surface area and more active sites for dye molecules to attach.[57]

3.2.6. Effect of dye solution pH on adsorption. pH of the dye solution is an important factor[58] that can affect dye removal by bringing a change in the surface charges. Usually, at low pH, the removal efficiency of anionic dye increases, and at high pH, the removal efficiency of cationic dye increases.[59] In general, acidic pHs are not suitable for the adsorption of cationic dyes as lower removal efficiency was noted at pH 3 for MB, MG, and RhB of 17 ± 3, 36 ± 3, and 47 ± 3%, respectively. It was discovered that decreasing pH reduced dye removal effectiveness because dye molecules competed with H^+ for accessible active sites at lower pH levels.[60] In Fig. 6d, the removal efficiency at contact time is demonstrated for the three selected dyes at different pH conditions. MB and RhB showed higher removal efficiency of 68 ± 3% and 74 ± 4%, respectively, at basic pH. The study found that increasing the initial pH improves the efficacy of MB and RhB dye adsorption, with the highest removal efficiency achieved around pH 11, which agrees with many researchers.[61] Meanwhile, the highest removal efficiency of 91 ± 3% was observed for MG dye adsorption at a native pH 6, as indicated in other research as well.[7] MG dye becomes colorless at high pH due to the interaction between the cationic MG and the hydroxyl ions in the aqueous solution[62,63] (refer to Fig. S7† for pH study in different dyes concerning time with ON11-10@PSU membrane).

3.3. Adsorption kinetic studies of ON11@PSU-pad

Adsorption kinetics assesses the rate at which an adsorbate is absorbed over time at a given concentration, providing insights into the diffusion of the adsorbate into the pores and suggesting a potential sorption mechanism.[19] The pseudo-first-order (PFO) model, the linearized expression of the Lagergren pseudo-first-order rate equation,[64] is represented as eqn (3):

$$\log(q_e - q_t) = \log q_e - \frac{K_1 t}{2.303} \quad (3)$$

In this equation, q_e and q_t represent the amounts of adsorbate adsorbed at equilibrium and at time (t), respectively, while k_1 (min^{-1}) denotes the rate constant PFO model. The plots of $\log(q_e - q_t)$ against time for the pseudo-first-order model for all the selected dyes are presented in Fig. 7a. A significant discrepancy was observed between the tabulated values in Table 4, indicating that the PFO kinetic model is inadequate for describing the proposed adsorption behavior.

According to the pseudo-second-order (PSO) kinetic model, the adsorption occurs at two surface sites.[65] The linear fit model of PSO kinetics can be given in eqn (4):

$$\frac{1}{q_t} = \frac{1}{K_2 q_e^2} + \frac{1}{q_e} t \quad (4)$$

where k_2 (g mg^{-1} min^{-1}) is the rate constant of the PSO model. The plot of t/q_t *vs.* time is plotted in Fig. 7b. The results, as indicated in Table 4 shows, with high correlation coefficient values (R^2 > 0.99 for all the selected dyes), confirm that the experimental data aligned well with the PSO kinetic model showcasing the dye adsorption behavior onto the ON11@PSU-pad.

This kinetics indicates a heterogeneous adsorbent surface, where different active sites have different affinities for the adsorbate. This is based on the assumption that the rate-limiting step could involve chemisorption, where valency forces come into play by sharing or exchanging electrons between the sorbent and sorbate.[66]

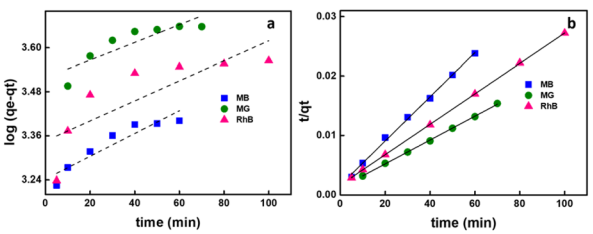

Fig. 7 (a) Pseudo-first-order and (b) pseudo-second-order kinetics for ON11-10@PSU-pad dye adsorption.

Table 4 Summary of kinetic model constants for MB, MG, and RhB dye adsorption on ON11@PSU

Kinetic models		MB	MG	RhB
PFO	k_1 (min^{-1})	0.046	0.0467	0.0062
	q_e (mg g^{-1})	65.831	61.384	28.383
	R^2	0.78	0.77	0.59
PSO	k_2 (g mg^{-1} min^{-1})	2.8×10^{-4}	1.18×10^{-4}	4.05×10^{-5}
	q_e (mg g^{-1})	20 063.6	19 889.53	3902.82
	R^2	0.99	0.99	0.99

3.4. Reusability of ON11@PSU-pad

The reusability of ON11@PSU-pad was evaluated using MG dye over three cycles, as seen in Fig. 5c. For the recyclability test, membranes were submerged in ethanol and stirred for 10–15 minutes or until the dye desorption occurred. This method desorbed MG dye in ethanol, enabling the membrane to be regenerated and recycled.[67] The removal efficiency remained consistent (~90%) across the cycles. However, the structural integrity of the membrane diminished with subsequent reuse, primarily due to disintegration caused by repeated washing (refer to ESI Fig. S8† for recyclability test effect on structural integrity of membrane pad).

3.4.1. Long-term stability of ON11@PSU-pad for dye removal. Performance longevity tests were conducted toward the ON11-10@PSU-pad for repeated dye removals, as stated in the hereupon section, using repeated reusability tests. Nevertheless, some structural instabilities did occur that caused the need for attention toward the membrane. Following a few runs, there had been slight membrane deformation, basically owing to physical strain from repeated washings as well as dexterity; the delayed gradual disintegration – probably acting from repetitive expansion as well as remission of the membrane during the processes of dye adsorption–desorption – led to a gradual degradation of their mechanical integrity. These modifications may affect the performance of membranes in long-term applications, as additional cycles may result in a loss of efficiency. Despite this, the ON11@PSU-pad remains a potential choice for dye removal applications because of its ability to maintain high removal efficiency in the short term. Further optimization of the membrane material or surface alterations may improve its long-term stability.

The membrane pads can be utilized in modular treatment systems, such as layered filter systems, allowing for easy replacement and reusability. Our study demonstrated the recyclability of ON11@PSU-pad across multiple cycles, highlighting its cost-effectiveness and sustainability for repeated use. While this study is focused on cationic dyes, future functionalization of the membrane or testing with mixed dye systems could enable selective adsorption capabilities, enhancing its use in diverse wastewater streams. Beyond dye removal, the membranes could be tailored for selective adsorption of other pollutants, including heavy metals, pharmaceuticals, or pesticides, by modifying the carbon nanospheres or polymer matrix.

The PSU matrix used in ON11@PSU membranes is a non-biodegradable polymer; however, the integration of bio-based ON11 enhances the sustainability of the composite by utilizing biowaste, thereby aligning with circular economy principles. Using green solvents, natural additives, or bio-sourced materials during membrane fabrication could improve their eco-friendliness and biodegradability.[68,69] While PSU was selected for its superior mechanical strength, thermal stability, and compatibility with ON11, future research will focus on incorporating ON11 into biodegradable polymer matrices. This approach aims to enhance the environmental sustainability of the membranes without compromising their performance. Additionally, strategies for recycling or repurposing PSU-based membranes after their functional lifetime could further mitigate environmental impact.

3.5. Dye adsorption mechanism on ON11@PSU-pad

The dye removal mechanism using the ON11@PSU-pad membrane pad is mainly based on the adsorption phenomenon. The surface charge of the membrane and its pore surface greatly depends on the adsorption performance.[70,71] The zeta potential of carbon nanomaterial (ON11) is around −19.6 mV (refer to ESI Fig. S9†), and the PSU membrane[72] surface is about −18 mV. The combined impact of these two significantly improves the total ON11@PSU-pad membrane surface and pore charge. SEM examination also shows that the nanomaterial is effectively dispersed across the membrane and pore surfaces (refer to ESI Fig. S10† for N_2 adsorption–desorption curve and pore size distribution of ON11). The surface area, average pore diameter, and pore volume calculated from BET were 423.26 m^2 g^{-1}, 1.26 nm, and 0.26 cm^3 g^{-1}, respectively. BJH pore diameter was around 4.5 nm aligning with the mesoporous nature of the ON11. Adsorption occurs when the dye comes into contact with the negatively charged membrane surface, as the dye pollutant used in this investigation is cationic (MB, MG, RhB). This oppositely charged dye and membrane strengthened the electrostatic attraction between these two, primarily facilitating the adsorption procedure.[73,74] For MB, MG, and RhB, the dye removal efficiency using the membrane pad is 67 ± 5%, 98 ± 3%, and 92 ± 3%, respectively, at 60 min contact time using 60 μm ON11-10@PSU-pad in native pH for 2.5 ppm concentration.

A graphical representation is described in Fig. 8 to better understand the possible dye adsorption mechanism using the ON11@PSU membrane pad. In addition to electrostatic interactions, the dye adsorption mechanism involves hydrogen bonding, van der Waals forces, and π–π stacking interactions[19,61] between the dye molecules and membrane surface. The selectivity of the prepared ON11@PSU pads towards different dyes depends on factors like pore size distribution and molecular sieving effect, polymer filler interaction and transport pathways, adsorption-dominated separation, and molecular interactions. The high surface area of the ON11 with oxygen-containing functional groups causes π–π interactions, enabling strong adsorption with dye molecules. This, in turn, enhances the retention of cationic dyes due to the electrostatic attraction with negatively charged ON11 and ON11@PSU membranes. The interfacial voids are created in the PSU membrane due to the dispersion of porous fillers, which visualizes improved permeability with controlled pore connectivity. The pore structure of the ON11 CNS incorporated into the PSU membrane plays a crucial role in dye adsorption. BET analysis revealed a mesoporous framework ranging from 2 to 10 nm (refer to ESI Fig. S10b†), which is well-suited for the molecular dimensions of MG (~1.8 nm), RhB (~1.5–1.7 nm), and MB (~1.43 nm). These mesopores facilitate efficient dye diffusion and adsorption, while micropores may enhance surface interactions. The high removal efficiency of MG and RhB indicates stronger π–π stacking and electrostatic attractions, whereas MB

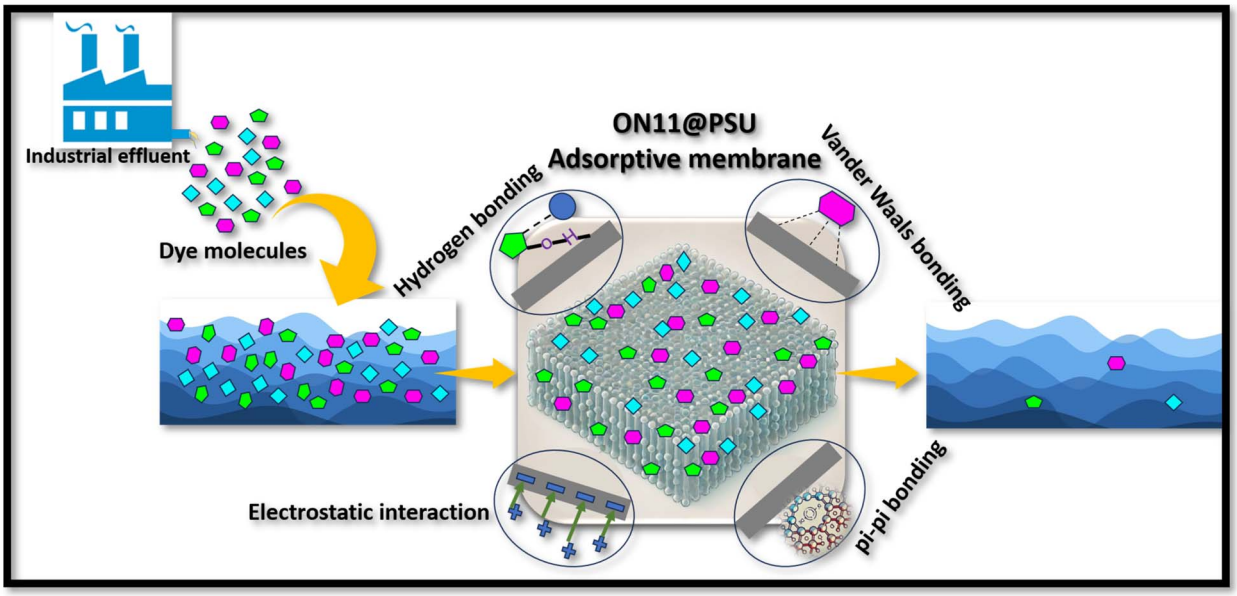

Fig. 8 Plausible adsorption mechanism of organic dyes onto ON11@PSU-pad.

likely exhibits weaker adsorption and faster diffusion, possibly due to its lower hydrophobic affinity. All of the mechanisms involved in the adsorption process confirmed the efficient adsorption of dye using ON11@PSU-pad from water as soon as it became immersed in the polluted water. Additionally, this membrane-based adsorption process has several advantages over solely using nanomaterials for adsorption. Nanomaterials have certain drawbacks, such as the difficulty of removing spent nanomaterials after water treatment, despite the fact that it is effective. However, the incorporation of nanomaterials into the membrane to create a MMM helps to hold the nanomaterial without compromising its adsorption effectiveness by providing a large surface area for contact with dye, and removal is also simple and feasible for reusability after treatment (see reusability study). These benefits prompted us to create a membrane pad that would more effectively and hassle-free adsorb the water contaminant.

4. Conclusion and future perspectives

In this study, we have developed a bio-based, onion peel-derived nanomaterial ON11-incorporated mixed matrix membrane (ON11@PSU) that demonstrates high efficacy in adsorbing cationic dyes like MB, MG, and RhB. This composite membrane proves to be a promising candidate for wastewater treatment. Incorporating *Allium cepa*-derived carbon nanospheres significantly enhanced the adsorption efficiency, with optimal dye removal achieved at a membrane thickness of 60 μm. The dye removal efficiency was evaluated by varying membrane thickness, layer of membrane pad, dye concentration, ON11 dosage, contact time, and solution pH. The 60 μm membranes exhibited enhanced adsorption, with maximum removal efficiencies of 67 ± 5% for MB, 98 ± 3% for MG, and 92 ± 3% for RhB at 2.5 ppm dye concentrations. By increasing the number of membrane pads, the removal efficiency also increases as surface area increases. Kinetic studies suggest that the adsorption process follows a pseudo-second-order model, indicating a chemisorption-driven mechanism. The membrane maintained strong performance through several reuse cycles, though further material refinement is needed to improve its structural stability for long-term applications.

The limitations of this study include the diminished structural stability of ON11@PSU after repeated use as the physical wear resistance of the membrane needs improvement to enhance durability for long-term applications. Challenges in scaling up production using eco-friendly methods and the use of a non-biodegradable polymer matrix is required for future material optimization. Future work can focus on stability enhancement and expanding its application in mixed system of dyes and strengthening the membranes for long term applications. Furthermore, our future research will lead to the scaling up of membrane production utilizing environmentally friendly, cost-effective processes for real-world applications. This work aligns with circular economy concepts and provides a promising direction for sustainable water treatment technologies using bio-waste.

Data availability

The data supporting this article have been included as part of the ESI.†

Author contributions

Aman Sharma: conceptualization, investigation, methodology, data curation, formal analysis, writing—draft manuscript, visualization, writing—original draft, revision of manuscript

and editing, writing—review and editing. Soumi Datta: revision of manuscript and editing, visualization, formal analysis, reviewing. R. K. Sanjana: data curation, investigation. B. M. Pooja: data curation, investigation. Suryasarathi Bose: reviewing, validation, and final approval of the manuscript to be published. Gurumurthy Hegde: revision of manuscript and editing, supervision, validation, formal analysis, reviewing, and final approval of the manuscript to be published.

Conflicts of interest

There are no conflicts to declare.

References

1 S. S. Vedula and G. D. Yadav, *J. Indian Chem. Soc.*, 2022, **99**, 100263.
2 J. Fang, Y. Chen, C. Fang and L. Zhu, *Sep. Purif. Technol.*, 2022, **281**, 119876.
3 A. Sharma, S. Sunny, J. Arulraj and G. Hegde, *Nano Express*, 2024, **5**, 022002.
4 J. Cheng, C. Zhan, J. Wu, Z. Cui, J. Si, Q. Wang, X. Peng and L.-S. Turng, *ACS Omega*, 2020, **5**, 5389–5400.
5 I. Khan, K. Saeed, I. Zekker, B. Zhang, A. H. Hendi, A. Ahmad, S. Ahmad, N. Zada, H. Ahmad, L. A. Shah, T. Shah and I. Khan, *Water*, 2022, **14**, 242.
6 D. Pathania, S. Sharma and P. Singh, *Arabian J. Chem.*, 2017, **10**, S1445–S1451.
7 M. Abewaa, A. Mengistu, T. Takele, J. Fito and T. Nkambule, *Sci. Rep.*, 2023, **13**, 14701.
8 S. Srivastava, R. Sinha and D. Roy, *Aquat. Toxicol.*, 2004, **66**, 319–329.
9 A. Bazan-Wozniak, A. Jędrzejczak, R. Wolski, S. Kaczmarek, A. Nosal-Wiercińska, J. Cielecka-Piontek, S. Yagmur-Kabas and R. Pietrzak, *Molecules*, 2024, **29**, 1412.
10 J. Sharma, S. Sharma, U. Bhatt and V. Soni, *J. Hazard. Mater. Lett.*, 2022, **3**, 100069.
11 H. Li, T. Li, W. Shi, Y. Tian, J. Liu and X. Qin, *React. Funct. Polym.*, 2022, **170**, 105135.
12 D. Teng, Y. Xu, T. Zhao, X. Zhang, Y. Li and Y. Zeng, *J. Hazard. Mater.*, 2022, **425**, 128004.
13 N. Benosmane, B. Boutemeur, S. M. Hamdi and M. Hamdi, *Appl. Water Sci.*, 2022, **12**, 104.
14 Y. Kang, J. Jang, Y. Lee and I. S. Kim, *Desalination*, 2022, **524**, 115462.
15 E. Shokri, R. Yegani and A. Akbarzadeh, *Appl. Clay Sci.*, 2017, **144**, 141–149.
16 W. Zhu, Z. Wu, S. Zhao, F. Lv, Y. Zhang and S. Guo, *Chem. Eng. Sci.*, 2023, **280**, 119009.
17 C.-H. Lin, C.-H. Gung, J.-Y. Wu and S.-Y. Suen, *J. Taiwan Inst. Chem. Eng.*, 2015, **51**, 119–126.
18 P. M. Thabede, *Appl. Sci.*, 2023, **13**, 10511.
19 A. Sharma, J. M. Shivanna, A. N. Alodhayb and G. Hegde, *Nanoscale Adv.*, 2024, **6**, 3199–3210.
20 B. Krishnappa, S. Saravu, J. M. Shivanna, M. Naik and G. Hegde, *Environ. Sci. Pollut. Res. Int.*, 2022, **29**, 79067–79081.
21 V. Molahalli, A. Shetty, A. Sharma, K. Bijapur, G. Soman and G. Hegde, in *Nanoparticles and Plant-Microbe Interactions*, Elsevier, 2023, pp. 35–68.
22 S. Supriya, G. Sriram, Z. Ngaini, C. Kavitha, M. Kurkuri, I. P. De Padova and G. Hegde, *Waste Biomass Valorization*, 2019, **11**, 3821–3831.
23 H. Yang, R. Yan, H. Chen, D. H. Lee and C. Zheng, *Fuel*, 2007, **86**, 1781–1788.
24 M. S. Jyothi, M. Padaki, R. G. Balakrishna and R. K. Pai, *J. Mater. Res.*, 2014, **29**, 1537–1545.
25 H. L. Richards, P. G. L. Baker and E. Iwuoha, *J. Surf. Eng. Mater. Adv. Technol.*, 2012, **02**, 183–193.
26 S. Modi, V. K. Yadav, N. Choudhary, A. M. Alswieleh, A. K. Sharma, A. K. Bhardwaj, S. H. Khan, K. K. Yadav, J.-K. Cheon and B.-H. Jeon, *Materials*, 2022, **15**, 2393.
27 R.-F. Segundo, M. De La Cruz-Noriega, N. Milly Otiniano, S. M. Benites, M. Esparza and R. Nazario-Naveda, *Molecules*, 2022, **27**, 625.
28 A. M. Alosaimi, *Polymers*, 2021, **13**, 2792.
29 M. Arulkumar, P. Sathishkumar and T. Palvannan, *J. Hazard. Mater.*, 2011, **186**, 827–834.
30 V. S. Bhat, S. G. Krishnan, T. J. Jayeoye, T. Rujiralai, U. Sirimahachai, R. Viswanatha, M. Khalid and G. Hegde, *J. Mater. Sci.*, 2021, **56**, 13271–13290.
31 V. S. Bhat, S. Supriya and G. Hegde, *J. Electrochem. Soc.*, 2019, **167**, 037526.
32 L. Mei and G. Guan, *Nano TransMed*, 2023, **2**, e9130017.
33 F.-G. Tseng, D. Bhalothia, K.-H. Lo, C.-H. Syu, Y.-C. Chen, A. Sihag, C.-W. Wang, H.-Y. T. Chen and T.-Y. Chen, *Energy Adv.*, 2024, **3**, 1283–1292.
34 X. Zhang, X. Wang, T. Cheng and Q. Lin, *J. Mol. Liq.*, 2023, **390**, 123091.
35 H. M. Abbas, R. M. Kamel, M. E. A. Ali, A. H. Atta, H. M. A. Hassan and A. Shahat, *Desalin. Water Treat.*, 2020, **193**, 57–63.
36 P. G. Ingole, S. Y. Sawant, N. P. Ingole, R. R. Pawar, H. C. Bajaj, K. Singh, M. H. Cho and H. K. Lee, *Membr. Water Treat.*, 2016, **7**, 477–493.
37 K. Parveen, U. Rafique and M. J. Akhtar, *J. Environ. Health Sci. Eng.*, 2022, **20**, 757–774.
38 M. Manoukian, H. Fashandi and H. Tavakol, *Mater. Res. Express*, 2019, **6**, 055313.
39 X. Zhao, C. Wu, D. Dai, J. Ren, T. Li and S. Ling, *iScience*, 2023, **26**, 107290.
40 E. S. Mansor, H. Ali and A. Abdel-Karim, *Colloid Interface Sci. Commun.*, 2020, **39**, 100314.
41 L. Zhang, H. Zhang, W. Guo and Y. Tian, *Appl. Clay Sci.*, 2014, **94**, 85–93.
42 M. Farooq, S. Shujah, K. Tahir, S. Nazir, A. Ullah Khan, Z. M. Almarhoon, V. Jevtovic, H. S. Al-Shehri, S. Tasleem Hussain and A. Ullah, *Inorg. Chem. Commun.*, 2022, **136**, 109189.
43 J. Hou, Y. Chen, W. Shi, C. Bao and X. Hu, *Appl. Surf. Sci.*, 2020, **505**, 144145.
44 G. Yang, H. Gao, Q. Li and S. Ren, *RSC Adv.*, 2021, **11**, 15921–15926.

45 G. L. Kyriakopoulos, K. Tsimnadis, I. Sebos and Y. Charabi, *Crystals*, 2024, **14**, 742.
46 S. Dutta, B. Gupta, S. K. Srivastava and A. K. Gupta, *Mater. Adv.*, 2021, **2**, 4497–4531.
47 Z. Eren and F. N. Acar, *Desalination*, 2006, **194**, 1–10.
48 E. Rápó and S. Tonk, *Molecules*, 2021, **26**, 5419.
49 C. Tejada-Tovar, Á. Villabona-Ortíz and Á. D. Gonzalez-Delgado, *Water*, 2021, **13**, 1382.
50 N. K. Mondal and S. Kar, *Appl. Water Sci.*, 2018, **8**, 157.
51 A. Khodabandehloo, A. Rahbar-Kelishami and H. Shayesteh, *J. Mol. Liq.*, 2017, **244**, 540–548.
52 A. E. Ofomaja, *Biochem. Eng. J.*, 2008, **40**, 8–18.
53 M. Naghizade Asl, N. M. Mahmodi, P. Teymouri, B. Shahmoradi, R. Rezaee and A. Maleki, *Desalin. Water Treat.*, 2016, **57**, 25278–25287.
54 C. Osagie, A. Othmani, S. Ghosh, A. Malloum, Z. Kashitarash Esfahani and S. Ahmadi, *J. Mater. Res. Technol.*, 2021, **14**, 2195–2218.
55 B. P. Chang, A. Gupta and T. H. Mekonnen, *Chemosphere*, 2021, **282**, 131062.
56 L. Ceroni, S. Benazzato, S. Pressi, L. Calvillo, E. Marotta and E. Menna, *Nanomaterials*, 2024, **14**, 522.
57 M. Saghanejhad Tehrani and R. Zare-Dorabei, *RSC Adv.*, 2016, **6**, 27416–27425.
58 S. Lu, Y. Yang, X. Su, K. Yu and X. Wang, *Sustainability: Sci. Pract. Policy*, 2022, **14**, 10935.
59 Y. Zhou, J. Lu, Y. Zhou and Y. Liu, *Environ. Pollut.*, 2019, **252**, 352–365.
60 S. N. Taqui, C. S. Mohan, B. A. Khatoon, M. E. M. Soudagar, T. M. Y. Khan, M. A. Mujtaba, W. Ahmed, A. Elfasakhany, R. Kumar and C. I. Pruncu, *Biomass Convers. Biorefin.*, 2023, **13**, 9119–9130.
61 A. A. E. A. Elfiky, M. F. Mubarak, M. Keshawy, I. E. T. E. Sayed and T. A. Moghny, *Environ. Sci. Pollut. Res. Int.*, 2023, **30**, 79091–79105.
62 S. T. Kadhum, G. Y. Alkindi and T. M. Albayati, *Desalin. Water Treat.*, 2021, **231**, 44–53.
63 A. R. Fischer, P. Werner and K.-U. Goss, *Chemosphere*, 2011, **82**, 210–214.
64 M. I. Khan, S. Akhtar, S. Zafar, A. Shaheen, M. A. Khan, R. Luque and A. U. Rehman, *Materials*, 2015, **8**, 4147–4161.
65 B. Baheri, R. Ghahremani, M. Peydayesh, M. Shahverdi and T. Mohammadi, *Res. Chem. Intermed.*, 2016, **42**, 5309–5328.
66 Y. S. Ho and G. McKay, *Process Biochem.*, 1999, **34**, 451–465.
67 J. Saleem, Z. K. B. Moghal, S. Pradhan, A. Hafeez, M. Shoaib, J. Alahmad and G. McKay, *Polymers*, 2024, **16**, 1459.
68 Y. X. Foong, L. H. Yew and P. V. Chai, *Mater. Today*, 2021, **46**, 2092–2097.
69 M. Ehsani, D. Kalugin, H. Doan, A. Lohi and A. Abdelrasoul, *Appl. Sci.*, 2022, **12**, 12837.
70 S. Dutta, A. Misra and S. Bose, *Nanoscale*, 2024, **16**, 5188–5205.
71 M. Elimelech, W. H. Chen and J. J. Waypa, *Desalination*, 1994, **95**, 269–286.
72 P. Van der Meeren, H. Saveyn, S. Bogale Kassa, W. Doyen and R. Leysen, *Phys. Chem. Chem. Phys.*, 2004, **6**, 1408–1412.
73 S. Dutta, R. Sen Gupta, K. Manna, S. Safikul Islam and S. Bose, *Chem. Eng. J.*, 2023, **472**, 145008.
74 S. Dutta, B. G. M. Patel, Y. Singh, G. Hegde and S. Bose, *J. Membr. Sci.*, 2024, **694**, 122422.